Metabolism Clinical and Experimental 95 (2019) 8–20

Contents lists available at ScienceDirect

Metabolism Clinical and Experimental

journal homepage: www.metabolismjournal.com

Basic Science

Systemic PPARγ deletion in mice provokes lipoatrophy, organomegaly, severe type 2 diabetes and metabolic inflexibility

Federica Gilardi *,[1], Carine Winkler, Laure Quignodon, Jean-Gael Diserens, Barbara Toffoli, Mariano Schiffrin, Chiara Sardella, Frédéric Preitner, Béatrice Desvergne **

Center for Integrative Genomics, Faculty of Biology and Medicine, University of Lausanne, CH-1015 Lausanne, Switzerland

ARTICLE INFO

Article history:
Received 27 November 2018
Accepted 12 March 2019

Keywords:
PPARγ
Lipodystrophy
In-depth metabolic exploration
Metabolic inflexibility
Type 2 diabetes

ABSTRACT

Background: The peroxisome proliferator-activated receptor γ (PPARγ) is a ligand-dependent transcription factor involved in many aspects of metabolism, immune response and development. Numerous studies relying on tissue-specific invalidation of the *Pparg* gene have shown distinct facets of its activity, whereas the effects of its systemic inactivation remain unexplored due to embryonic lethality. By maintaining PPARγ expression in the placenta, we recently generated a mouse model carrying *Pparg* full body deletion ($Pparg^{\Delta/\Delta}$), which in contrast to a previously published model is totally deprived of any form of adipose tissue. Herein, we propose an in-depth study of the metabolic alterations observed in this new model.

Methods: Young adult mice, both males and females analyzed separately, were first phenotyped for their gross anatomical alterations. Systemic metabolic parameters were analyzed in the blood, in static and in dynamic conditions. A full exploration of energy metabolism was performed in calorimetric cages as well as in metabolic cages. Our study was completed by expression analyses of a set of specific genes.

Main findings: $Pparg^{\Delta/\Delta}$ mice show a striking complete absence of any form of adipose tissue, which triggers a complex metabolic phenotype including increased lean mass with organomegaly, hypermetabolism, urinary energy loss, hyperphagia, and increased amino acid metabolism. $Pparg^{\Delta/\Delta}$ mice develop severe type 2 diabetes, characterized by hyperglycemia, hyperinsulinemia, polyuria and polydispsia. They show a remarkable metabolic inflexibility, as indicated by the inability to shift substrate oxidation between glucose and lipids, in both *ad libitum* fed state and fed/fasted/refed transitions. Moreover, upon fasting $Pparg^{\Delta/\Delta}$ mice enter a severe hypometabolic state.

Conclusions: Our data comprehensively describe the impact of lipoatrophy on metabolic homeostasis. As such, the presented data on $Pparg^{\Delta/\Delta}$ mice gives new clues on what and how to explore severe lipodystrophy and its subsequent metabolic complications in human.

1. Introduction

Adipose tissue is a plastic tissue central to metabolic health by virtue of both its fat-storage and endocrine roles; the extreme deviations of its mass are associated with severe pathological states. Obesity is a risk factor for metabolic syndrome associated with hyperglycemia, hypertension, hyperlipidemia, insulin resistance, and with increased risk for cardiovascular diseases and type-2 diabetes [1,2]. It is accompanied by pronounced alterations in the secretory profile of adipocytes and macrophages, resulting in chronic low-grade inflammation and subsequent adipocyte dysfunction [3–5]. Opposite to obesity, the lack of fat is called lipoatrophy. The most severe human form is the Berardinelli-Seip syndrome, which is a congenital generalized lipodystrophy provoked by mutations in *BSCL2* or in *AGPAT2* genes. Interestingly, lipodystrophic patients suffer from the same disorders as obese patients, including severe insulin resistance and type-2 diabetes [6,7]. A unifying model proposes that when adipose tissue expandability is exhausted, such as in the presence of excess of lipids (obesity) or of insufficient body fat capacity (lipodistrophy), lipids cannot be safely stored in ectopic fat and accumulate in ectopic tissues, promoting lipotoxicity, insulin resistance and apoptosis [8–10].

Abbreviations: BAT, brown adipose tissue; GTT, glucose tolerance test; HBA, β-Hydroxybutyric acid; ITT, insulin tolerance test; PPARγ, peroxisome proliferator-activated receptor γ; RER, respiratory exchange ratio; TG, triglycerides; TZDs, thiazolidinediones; WAT, white adipose tissue.

* Correspondence to: F. Gilardi, Faculty Unit of Toxicology, Forensic Toxicology and Chemistry Unit, University Center of Legal Medicine, Lausanne University Hospital - Geneva University Hospitals, Switzerland.

** Correspondence to: B. Desvergne, Center for Integrative Genomics, Genopode Building, CH-1015 Lausanne, Switzerland.

E-mail addresses: Federica.Gilardi@hcuge.ch (F. Gilardi), Beatrice.Desvergne@unil.ch (B. Desvergne).

[1] Present address: Faculty Unit of Toxicology, Forensic Toxicology and Chemistry Unit, University Center of Legal Medicine, Lausanne University Hospital - Geneva University Hospitals, Switzerland.

https://doi.org/10.1016/j.metabol.2019.03.003

Adipose tissue development relies on the activity of the adipogenesis master regulator peroxisome proliferator-activated receptor γ (PPARγ), a ligand-dependent transcription factor belonging to the nuclear receptor superfamily [11,12]. PPARγ has many other metabolic activities including insulin sensitization. Indeed, synthetic PPARγ ligands such as thiazolidinediones (TZDs) have proven to be potent in the treatment of type-2 diabetes [13,14]. Conversely, rare natural heterozygous mutations in humans affecting PPARγ binding or activity lead to the development of partial lipodystrophy, insulinoresistance, hepatic steatosis and hypertriglyceridemia [7,15]. Moreover, deletion of the PPARγ2 isoform in the obese *ob*/*ob* background [16] as well as the fat-specific PPARγ deletion in *Adipoq-Cre*/*Pparg*$^{fl/fl}$ mice (PPARγFKO mice) [17], invariably led to insulin resistance, hyperglycemia and hyperlipidemia, although resulting in different degrees of adipose tissue reduction. Likewise, the deletion of PPARγ in muscle confirmed its essential role to maintain whole body insulin sensitivity [18]. Finally, macrophage-specific deletion of PPARγ predisposed mice to diet-induced insulin resistance [19].

The effect of PPARγ whole body deletion could however not be explored due to placental defects [20,21]. In a first attempt to circumvent this embryonic lethality by preserving PPARγ expression in the placenta, Meox-Cre mice were bred with PPARγ-floxed mice [22]. However, this approach gave rise to high mosaicism with various degree of Cre-dependent recombination depending on tissues (our unpublished results and [23]).

By using Sox2-Cre mediated recombination instead to delete PPARγ in the embryo while maintaining its expression in the placenta [23], we obtained viable whole-body PPARγ null pups [21]. Whereas PPARγ null mice show post-natal lethality and delayed growth during the suckling period, they recover and grow properly after weaning. Importantly, throughout their life, PPARγ null mice exhibit a total lack of white and brown adipose tissue. In the present report, we analyzed the severe metabolic disorders that accompany this total lipoatrophy.

2. Materials and methods

2.1. Animals

Animal care and treatments were performed in agreement with the guidelines established by the European Community Council Directives (86/609/EEC) and were approved by the commission for animal experimentation of the cantonal veterinary services (Canton of Vaud). Whole body *Pparg* null mice were obtained as previously described [24]. Mice were kept in a 12:12 h light:dark cycle and fed a standard chow diet (cat. 3436, Kliba Nafag, Kaiseraugst, Switzerland) with water *ad libitum*. For growth curves *Pparg*$^{\Delta/\Delta}$ and littermate control males and females (N = 5–10) were distributed among cages as random blocks of 1 *Pparg* null and 2 control mice. Random blocking was also used in all experiments.

2.2. Mouse embryonic fibroblasts

MEFs were isolated from E13.5 embryos. Briefly, after removal of head and internal organs, embryos were minced and incubated for 20 min at 37 °C in 0.25% Trypsin-EDTA. Cell suspensions were centrifuged, suspended with cell culture media (DMEM/F-12 supplemented with 10% FBS, 20 mM glutamine, and penicillin/streptomycin), plated in P100, and cultured at 37 °C and 5% CO2. Cells were differentiated *in vitro* as previously reported [25], with or without rosiglitazone (0.5 μM). Differentiated MEFs were fixed in 4% paraformaldehyde and stained with 0.3% Oil-Red-O (Sigma) for 10 min.

2.3. Clinical parameters

Resistin and leptin were measured using the Luminex technology (Bioplex, Bio-Rad). Plasma and urine biochemical parameters were evaluated on a Cobas C111 analyzer (Roche Diagnostics, Rotkreuz, Switzerland) at the Mouse Metabolic Evaluation Facility of the University of Lausanne. Insulin levels were measured with the Mercodia Ultrasensitive insulin ELISA (Mercodia AB, Sweden).

2.4. Body composition

Analyses were performed in duplicate for each mouse with the EchoMRI™ qNMR system (Echo Medical Systems, Houston, TX, USA) under isoflurane anesthesia at the Mouse Metabolic Evaluation Facility (MEF) of the University of Lausanne.

2.5. Body temperature

The temperature was measured in 12 weeks old females (N = 6) using a rectal probe (Bioseb) after 4 days of acclimation.

2.6. Glucose metabolism

GTT was performed in 10–12 weeks old male and female control and *Pparg*$^{\Delta/\Delta}$ mice (N = 8). After 16 h of fasting, glucose (2 g/kg) was injected intraperitoneally. Blood was collected from the tail vein at 0, 15, 30, 60 and 120 min after the injection and glycemia was evaluated by the use of a glucometer (Bayer Breeze 2, Canada). For the ITT, 12 weeks old male and female mice (N = 3–6 per group) were fasted 6 h and then injected intraperitoneally with insulin (0.6 U/Kg). Blood glucose was measured at 0, 15, 30 and 60 min after insulin injection.

2.7. Indirect calorimetry

Indirect calorimetry was performed in 12 weeks old mice placed in individual chambers in a 12 cages CLAMS system (Columbus Instruments, OH, USA), placed in a temperature-controlled chamber. For *ad libitum* measurements, CO_2 production, locomotor activity, food and water intake were recorded during 2 cycles of 24-h, with unrestricted food access (N = 6). For the response to feeding-fasting-refeeding transitions, indirect calorimetry measurements included a full day in the *ad libitum* condition, followed by an overnight (16 h) fasting and a diurnal refeeding period (N = 3; results replicated in 6 independent cohorts of both males and females). For thermoneutrality experiments, calorimetry measurements were recorded during three consecutive intervals of 24 h: a first cohort (N = 3) was put at ambient temperature at 23 °C, then 32 °C, then 33 °C; a second independent cohort (N = 3) was put at ambient temperature at 23 °C, then 32 °C, then 30 °C. Fermentation artifacts were prevented by trapping urine into diaper strips placed underneath the chamber floors. Moreover, during thermoneutrality experiments, mice were transferred every 24 h at the time of temperature transitions into new experimental cages conditioned with their own smell.

2.8. Urine/feces analyses

Mice were acclimated to metabolic cages (Tecniplast 3600 M021). Then urine and feces were collected over three consecutive intervals: 1) 24 h with food *ad libitum*, 2) first 5 h of fasting, and 3) successive 9 h of fasting (N = 7). The energy content of food and feces was measured with a calorimetric bomb (IKA C200, Staufen, Germany). Metabolizable energy was estimated by subtracting the 24 h hour energy loss in both urine (approximated as the energy lost as glucose, TGs, NEFAs, ketone bodies, proteins and urea), and in feces, to the 24 h feeding gross energy (16.1MJ/kg of chow diet).

2.9. Histology and morphometry

After dissection organs were fixed 4 h in 4% PFA – PBS solution at 4 °C and were paraffin embedded. Paraffin sections of 4 μm thickness were made and stained with Hematoxylin-Eosin. For cryosections, organs were embedded in OCT (Sakura, Torrance, CA) and frozen on dry-ice.

For β-cell mass quantification, paraffin pancreatic sections were stained with anti-insulin antibody (dil 1:400, AO564, Dako). β-cell mass was calculated by measuring β-cell surface area using ImageJ software in 5–8 sections per pancreas and 4–5 pancreas per group. β-cell mass was extrapolated based on individual pancreas weight.

2.10. Protein expression

Proteins were extracted from frozen gastrocnemius using M-PER lysing buffer (78501) with added protease and phosphatase inhibitors (78426, 78429 Thermofisher). Western blot was performed with standard procedures, with the following antibodies (Akt (9272) and Phospho-Akt (9271 Cell Signaling)). Chemiluminescence was detected with SuperSignal West Pico (Pierce). Blots were exposed digitally using the Fusion FX system (Vilber) and bands were quantified using ImageJ.

2.11. Real-time quantitative PCR

Total RNA was isolated after homogenisation in TRI-Reagent (Ambion, Thermo Fisher Scientific Inc.) and extraction with RNeasy Mini Kit (Qiagen). Gene expression was analyzed by real-time quantitative PCR (FastStart Universal SYBR Green Master, Roche, USA) in a Stratagene MX3005P Detection System (Agilent Technologies, USA). Ribosomal protein S9 (*Rps9*) was used as housekeeping gene. Primer sequences are available upon request.

2.12. Statistical analyses

Values, expressed as mean ± SEM, were analyzed using Prism 5.0 (GraphPad Software, USA). Student's *t*-test, one-way or two-way ANOVA with Bonferroni post-test for multiple group comparisons were used to assess statistical significance. For leptin, resistin and insulin levels, data were log-transformed to show normal distribution for statistical analysis. A P value <0.05 was considered statistically significant.

3. Results

3.1. Generalized lipodystrophy and organomegalia in $Pparg^{\Delta/\Delta}$ mice

PPARγ whole body deletion was obtained in *Sox2-Cre*$^{tg/+}$;*Pparg*$^{\Delta/em\Delta}$ (called hereafter *Pparg*$^{\Delta/\Delta}$) mice, as previously described [24] and PPARγ expression was undetectable in spleen, liver, muscle, heart, colon, and brain (data not shown). Consistent with the fundamental role of PPARγ in adipogenesis [11,26], embryonic fibroblasts isolated from *Pparg*$^{\Delta/\Delta}$ embryos could not differentiate in adipocytes (Suppl. Fig. 1). Accordingly, *Pparg*$^{\Delta/\Delta}$ mice presented a generalized lipoatrophy, characterized by the complete absence of interscapular brown (BAT) and white (WAT) adipose tissues (Fig. 1A), as well as perirenal (Fig. 1B), mesenteric, perigonadal and subcutaneous WAT (Fig. 1C). Circulating adipokines such as resistin and adiponectin were not detectable, while leptin was extremely low in both male and female *Pparg*$^{\Delta/\Delta}$ mice (Fig. 1D and data not shown). While similar at birth, *Pparg*$^{\Delta/\Delta}$ mice showed post-natal growth retardation during the suckling period (Fig. 1E), during which around 30% of pups died. After weaning (3 weeks), the surviving pups started to grow faster, reaching the same body weight as control mice at 6–7 weeks and becoming heavier than their control littermates between 8 and 12 weeks of age (Fig. 1E), with no more lethality. Strikingly, the higher body weight in *Pparg*$^{\Delta/\Delta}$ mice was almost exclusively due to a very significant increase in lean mass, while fat content was barely augmented with body weight, in contrast to what was observed in littermate control mice (Fig. 1F, G) Indeed, adult *Pparg*$^{\Delta/\Delta}$ mice showed organomegaly affecting particularly the liver (Fig. 1C, H) but also intestine and spleen (Suppl. Fig. 2 and [27]), whereas heart and muscle masses were unchanged and reduced, respectively (Suppl. Fig. 2 and [28]). In absence of adipose tissue, *Pparg*$^{\Delta/\Delta}$ mice showed ectopic lipid deposition in the liver (Fig. 1I), but not in muscle [28].

3.2. Deep alterations of glucose homeostasis in $Pparg^{\Delta/\Delta}$ mice

At 10–12 weeks male and female *Pparg*$^{\Delta/\Delta}$ mice revealed a severe increase in plasma glucose, triglycerides (TGs) and free fatty acids (NEFAs) (Fig. 2A–C), an impaired glucose tolerance (Fig. 2D), and insulin resistance as suggested by the poor hypoglycemic response during an Insulin tolerance test (ITT) (Fig. 2E). Insulin action was also impaired in muscle, as demonstrated by the reduced phosphorylation of AKT upon insulin injection (Suppl. Fig. 3). Accordingly, fed *Pparg*$^{\Delta/\Delta}$ mice were highly hyperinsulinemic (Fig. 2F) with plasma insulin values 16-fold over control values. This hyperinsulinemia was accompanied by a massive enlargement of pancreatic islets (Fig. 2G) with a 6.4 fold increase in β-cell mass in *Pparg*$^{\Delta/\Delta}$ mice (Fig. 2H). These data suggest that β-cells are not exhausted by the very high chronic hyperglycemia.

3.3. Hyperphagia, hypermetabolism, and metabolic inflexibility in $Pparg^{\Delta/\Delta}$ mice

In order to get more insight into the metabolic phenotype of *Pparg*$^{\Delta/\Delta}$ mice we performed indirect calorimetry experiments. *Pparg*$^{\Delta/\Delta}$ mice were hypermetabolic with higher oxygen consumption (Fig. 3A) and consequently heat production (Fig. 3B), corresponding to a calculated 76% higher daily metabolic rate. *Pparg*$^{\Delta/\Delta}$ hypermetabolism was only partially accounted for by the higher lean, metabolically active mass (Fig. 3D). This hypermetabolism was accompanied by a remarkable hyperphagia (Fig. 3E). Interestingly, the circadian oscillations of heat production, food intake, and spontaneous locomotor activity (Fig. 3C, E, F) were qualitatively maintained, demonstrating a preserved daily rhythmicity, although the amplitude was dampened (night:day activity ratio was 2:1 in *Pparg*$^{\Delta/\Delta}$ mice as compared to 3,5:1 in controls; Fig. 3F).

The preferential use of substrates as energy source was assessed by calculating the respiratory exchange ratio (RER = VCO2/VO2). As expected, control mice presented typical circadian oscillations of the RER (Fig. 3G), while such rhythmicity was absent in *Pparg*$^{\Delta/\Delta}$ mice. Males and females exhibited a similar phenotype. Thus, *Pparg*$^{\Delta/\Delta}$ mice are not capable of switching between energy sources depending on the nutritional status, *i.e.* they are metabolically inflexible.

Collectively, these experiments underlined three major metabolic traits in *Pparg*$^{\Delta/\Delta}$ mice: hypermetabolism, hyperphagia, and metabolic inflexibility.

3.4. Hypermetabolism is not due to an alteration of thermoregulation in $Pparg^{\Delta/\Delta}$ mice

The fact that the lean, metabolically active mass did not fully account for the hypermetabolism of *Pparg*$^{\Delta/\Delta}$ mice (see Fig. 3D) suggested that other parameters might contribute to its onset. Notably, beside their metabolic phenotype, *Pparg*$^{\Delta/\Delta}$ present skin alterations, characterized by dryness, lack of the subcutaneous fat layer, short hair and progressive alopecia [24], which could have an effect on insulation ability. Thus, should thermoregulation be altered in *Pparg*$^{\Delta/\Delta}$ mice due to insulation impairment, the difference of metabolic rate between *Pparg*$^{\Delta/\Delta}$ and control mice would be expected to disappear in absence of cold stress, *i.e.* at thermoneutrality. To test this hypothesis, we successively exposed the mice to various ambient temperatures including room temperature (23 °C) and thermoneutrality (30 °C, 32 °C, and 33 °C). In both control and *Pparg*$^{\Delta/\Delta}$ mice, the metabolic rate decreased from 23 °C to 32 °C, but remained higher in *Pparg*$^{\Delta/\Delta}$ mice than in control mice (Fig. 3H). These data suggest that insulation does not play a significant role in the hypermetabolism in *Pparg*$^{\Delta/\Delta}$ mice. Interestingly, in both control and *Pparg*$^{\Delta/\Delta}$ mice, a further increase of the ambient temperature from

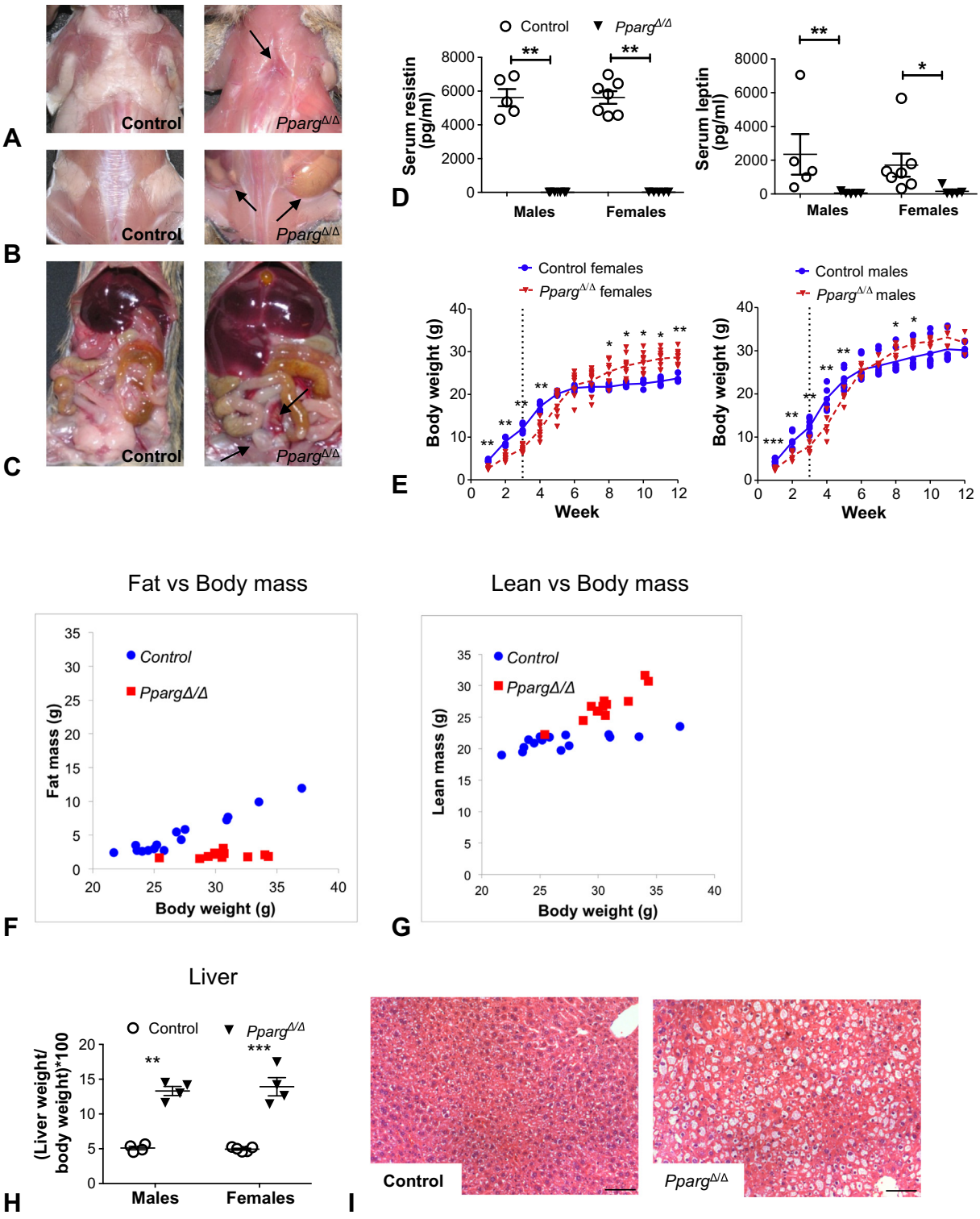

Fig. 1. Lipoatrophy and hepatomegaly in *Pparg*$^{\Delta/\Delta}$ mice. (A–B) Dorsal view after removal of the skin and (C) frontal view during dissection of 10 weeks old *Pparg*$^{\Delta/\Delta}$ mice and control littermates. Note the lack of visible (A) interscapular BAT and WAT, (B) perirenal WAT and (C) mesenteric and perigonadal WAT indicated by black arrows in *Pparg*$^{\Delta/\Delta}$ animal. (D) Serum levels of resistin and leptin measured in both male and female mice at 20 weeks. $N = 5$–7. (E) Growth curves in males and females between 1 and 12 weeks of age. Weaning at 3 weeks is highlighted by vertical dotted lines (F). Fat *vs* Body mass and (G) Lean *vs* Body mass in female *Pparg*$^{\Delta/\Delta}$ and aged-matched control mice (10–15 weeks). $N =$ 12–15. (H) Hepatomegaly in *Pparg*$^{\Delta/\Delta}$ mice at 10 weeks. (I) Representative images of liver sections stained with H&E in 10 weeks old males. Scale bar represents 100 μm. Individual values and mean ± SEM are plotted. *P < 0.05, **P < 0.01, ***P < 0.0001 *Pparg*$^{\Delta/\Delta}$ *vs.* control littermates.

32 ° to 33° did not result in further drop, but rather increased the metabolic rate. This suggests that in both genotypes 33 °C is beyond the upper limit of the thermoneutral zone, a temperature zone where active cooling is required to prevent hyperthermia with a paradoxical increases of the metabolic rate. Consistent with this notion, rectal temperature in *Pparg*$^{\Delta/\Delta}$ mice was slightly low at 23 °C, was normal at 30 °C but was higher at 32 and 33 °C (Fig. 3I). Control mice on the other hand maintained a constant temperature up to 33 °C. Overall, these results indicate that the hypermetabolism in *Pparg*$^{\Delta/\Delta}$ mice is not due to an impairement in insulation.

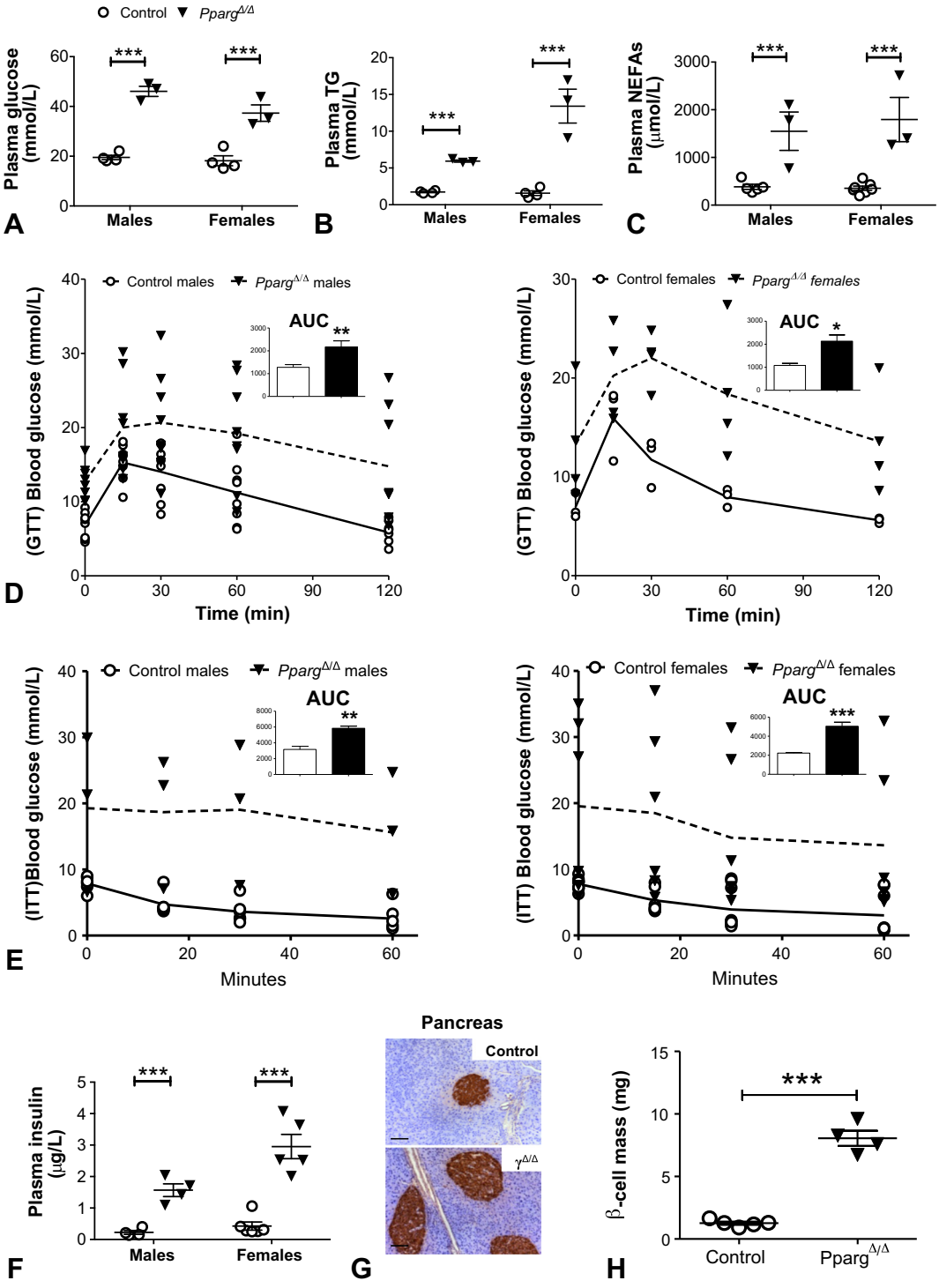

Fig. 2. Hyperglycemia, hyperlipidemia and insulin resistance in *Pparg*$^{\Delta/\Delta}$ mice. (A) Fed plasma glucose, (B) triglycerides (TG) and (C) NEFAs measured in both male and female mice at 10–12 weeks ($N = 3$–4). (D) GTT in both male and female mice at 10–12 weeks ($N = 8$). Area under the curve (AUC) was calculated from the GTT curve. (E) ITT in male (left panel) and female (right panel) mice at 12 weeks ($N = 3$–6). AUC was calculated from the ITT curve. (F) Fed plasma insulin evaluated in both sexes at 13 weeks of age ($N = 3$–6). (G) Representative images of insulin stained pancreatic sections from 20 weeks old female control and *Pparg*$^{\Delta/\Delta}$ mice. Scale bar represents 100 μm. (H) β-cell mass in 20 weeks old female control and *Pparg*$^{\Delta/\Delta}$ mice ($N = 4$–5). Individual values and mean ± SEM are plotted. *P < 0.05, **P < 0.01, ***P < 0.0001 *Pparg*$^{\Delta/\Delta}$ *vs.* control littermates.

3.5. Fasting intolerance in Pparg$^{\Delta/\Delta}$ *mice*

To further explore the metabolic phenotype related to energy homeostasis and metabolic flexibility, we submitted *Pparg*$^{\Delta/\Delta}$ mice to overnight (14 h) fasting.

Pparg$^{\Delta/\Delta}$ mice lost more body weight than controls (Fig. 4A). Although the fat loss was comparable among groups (2 g), fasting led to an almost complete depletion of fat mass in *Pparg*$^{\Delta/\Delta}$ mice. In addition, the loss of lean mass in *Pparg*$^{\Delta/\Delta}$ mice was twice that in control mice (Fig. 4B–C).

Fasting resulted in a two-third decrease of glycemia and a striking normalization of hyperinsulinemia in *Pparg*$^{\Delta/\Delta}$ mice (Fig. 4D, E). As expected, blood concentration of both ketone bodies (β-Hydroxybutyric acid (HBA)) and the ketogenic substrates NEFAs was increased upon fasting in control mice. In contrast, in *Pparg*$^{\Delta/\Delta}$ mice, NEFA and TG levels were high in the fed state but decreased upon fasting and the fasting-

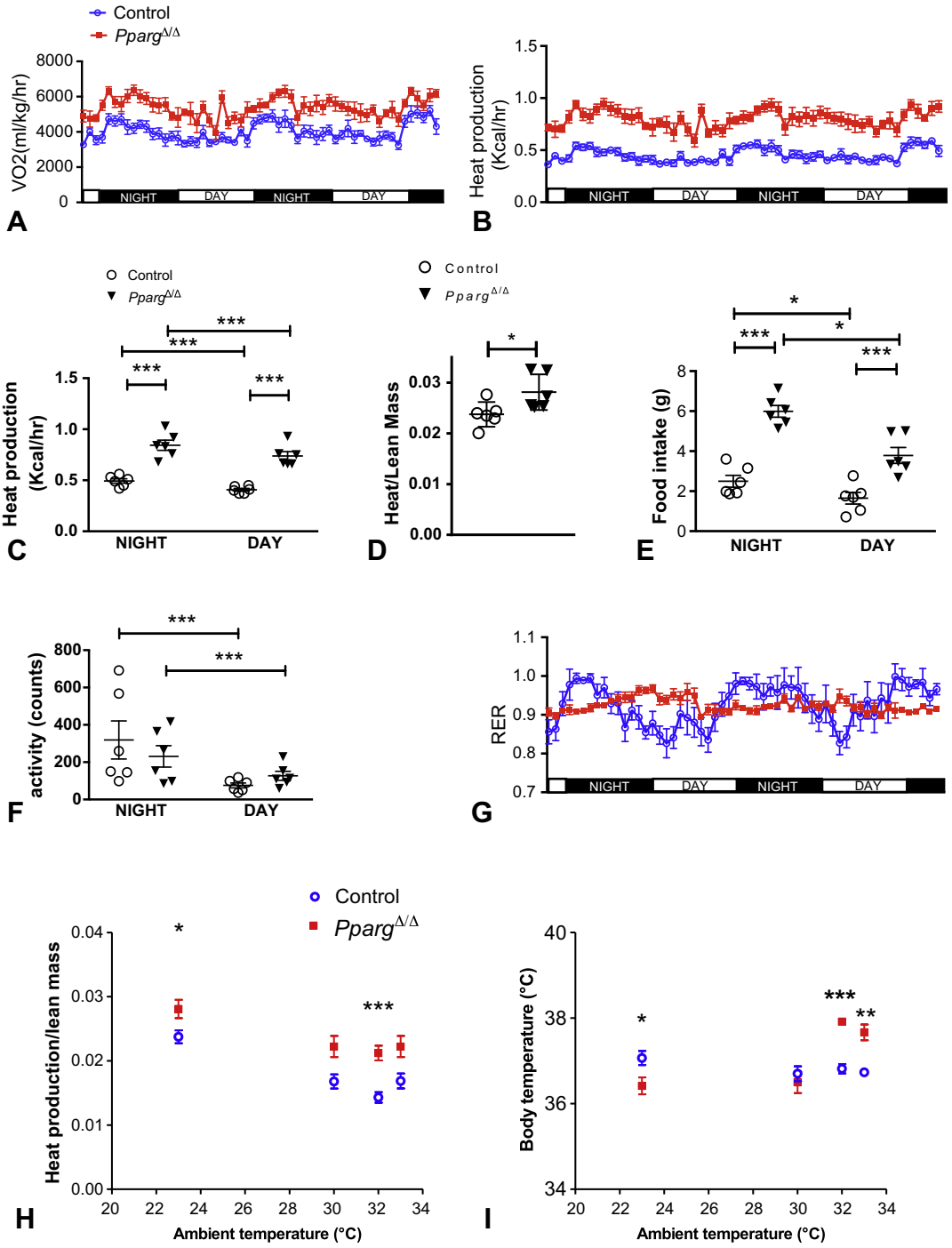

Fig. 3. Metabolic inflexibility and hypermetabolism in *Pparg*$^{\Delta/\Delta}$ mice. (A) Oxygen consumption and (B) heat production measured over 2 days in 12 weeks old control and *Pparg*$^{\Delta/\Delta}$ female mice. (C) Average heat production, (E) food intake and (F) locomotor activity during the dark (night) and light (day) phases. (D) Quantification of heat production normalized to lean mass. (G) Respiratory Exchange Ratio (RER) profile along 48 h ($N = 6$ female mice; similar results were obtained in 12 weeks old *Pparg*$^{\Delta/\Delta}$ and control littermate male mice). (H) Heat production normalized to lean mass, and (I) body temperature recorded at different environmental temperatures ($N = 3$–6). Mean ± SEM is shown. *P < 0.05, **P < 0.01, ***P < 0.0001 *Pparg*$^{\Delta/\Delta}$ *vs.* age-matched control littermates (student *t*-test).

induced increase in ketone bodies was accordingly blunted (Fig. 4F–H), suggesting that *Pparg*$^{\Delta/\Delta}$ mice are unable to normally adjust its metabolism during fasting.

3.6. Metabolic inflexibility and fasting-induced torpor in *Pparg*$^{\Delta/\Delta}$ mice

To further analyse this phenotype we assessed the metabolic response to a fed, overnight fasted, refed scheme by indirect calorimetry. In control mice, the RER rapidly dropped close to 0.7 during fasting (shift to lipid metabolism) and reciprocally rebounded close to 1.0 during refeeding (metabolic switch back to carbohydrates). In *Pparg*$^{\Delta/\Delta}$ mice, in contrast, the RER remained constant in the 0.8–0.9 range, until 9 h into the fasting (Fig. 5A). Strikingly, during the second part of the nocturnal fast, the VO_2 and heat production had dramatically dropped about 5-fold (Fig. 5B, C) and locomotor activity was suppressed (Fig. 5D), a state characteristic of fasting-induced torpor, a transient and spontaneously reversible hibernation-like, hypometabolic state. Upon

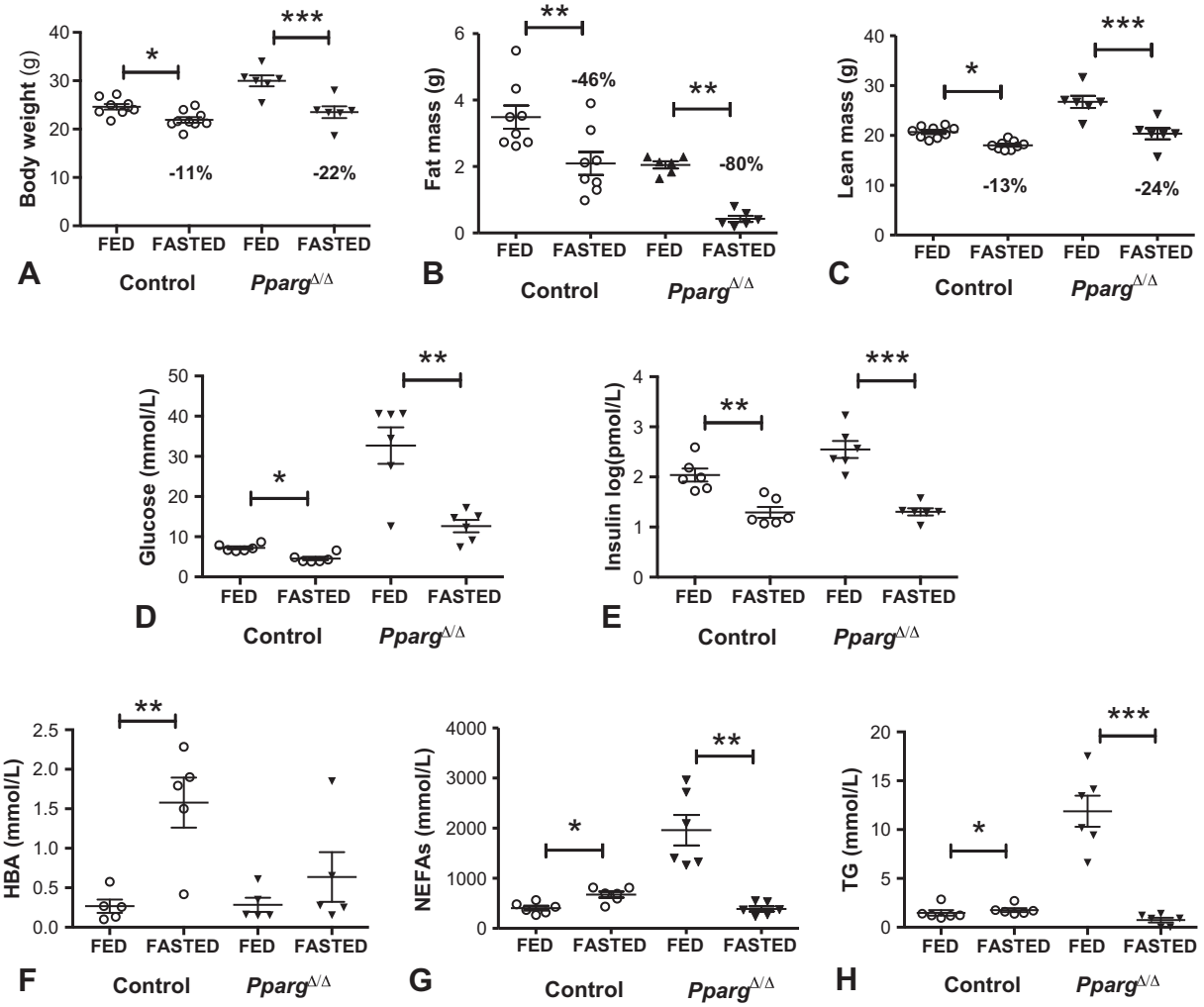

Fig. 4. *Pparg*$^{\Delta/\Delta}$ mice are intolerant to overnight fasting. Changes in (A) body weight (B) fat mass and (C) lean mass in response to overnight fasting in female *Pparg*$^{\Delta/\Delta}$ ($N = 6$) and control ($N = 8$) mice at 13–15 weeks. (D) Glucose, (E) insulin, (F) β-Hydroxybutyric acid (HBA), (G) Non Esterified Fatty Acids (NEFAs) and (H) Triglyceride (TG) levels in *Pparg*$^{\Delta/\Delta}$ and control female mice fed *ad libitum* or fasted overnight. ($N = 5$–9 per group). Individual values and the mean ± SEM are plotted. *P < 0.05, **P < 0.01, ***P < 0.0001 fasted *vs*. fed condition in the indicated genotype.

refeeding, *Pparg*$^{\Delta/\Delta}$ mice exited torpor and returned to the hypermetabolic state (Fig. 5A–C).

These results further support the notion that *Pparg*$^{\Delta/\Delta}$ mice are severely metabolically inflexible and intolerant to fasting.

3.7. Urinary energy loss and energy balance in *Pparg*$^{\Delta/\Delta}$ mice

Given our previous report of impaired renal function in *Pparg*$^{\Delta/\Delta}$ mice [29], we hypothesized that energy loss in urine may also contribute to energy store depletion and fasting-induced torpor in *Pparg*$^{\Delta/\Delta}$ mice.

To estimate energy loss in the feces and urine, we collected them during 24 h in the *ad libitum* fed state, followed by a second collection during 5 h fasting, and finally a third collection corresponding to the last 9 h of a 14 h fast. This protocol allowed distinguishing the early metabolic responses to fasting, when the metabolic rate was still in the normal range, from the late response, during fasting-induced torpor.

Pparg$^{\Delta/\Delta}$ mice are severely polyuric (Fig. 6A), consistent with the hyperglycemic and the diabetic state. The water loss is compensated by an important polydipsy (Fig. 6B). We evaluated the energy lost in urine by measuring the concentration of main metabolites in urine. In the fed state, *Pparg*$^{\Delta/\Delta}$ mice lose a very significant amount of glucose (2.6 g/24 h), but also TGs, NEFAs, ketone bodies (HBA) and proteins (Fig. 6C–G, 24 h fed). In addition, urea excretion was strikingly increased 4.7-fold, suggesting an elevation of aminoacid metabolism (Fig. 6H, 24 h fed). During fasting, the urinary loss progressively decreased in *Pparg*$^{\Delta/\Delta}$ mice for all substrates, including the ketone bodies (Fig. 6C–G, 5hr and 9 h fasting). This latter result is in stark contrast with control mice in which HBA urinary levels increased over the course of fasting (Fig. 6E), consistent with the fasting-induced increase in plasma ketone bodies (see also Fig. 4F).

In line with the polyphagia (Fig. 6I), during the normal feeding day, we also observed a 3-fold increase of the amount of feces produced by *Pparg*$^{\Delta/\Delta}$ mice (Fig. 6J), which resulted in a 3-fold higher energy loss compared to control mice (Fig. 6K), since feces density was not altered (Fig. 6L).

By recapitulating the various energy losses, one can calculate the portion of food energy available for body metabolism, *i.e*. the metabolizable energy (Fig. 6M). The energy loss in the feces produced by *Pparg*$^{\Delta/\Delta}$ mice accounted for *ca*. 25% of energy intake, similar to controls. In fact, the observed lower proportion of metabolizable energy in *Pparg*$^{\Delta/\Delta}$ mice (45% *vs* 75% in controls; Fig. 6M) was rather due to the very significant (30%) energy loss in urine, which thus likely contributes to inducing hyperphagia in *Pparg*$^{\Delta/\Delta}$ mice.

Finally, taking into account the higher energy intake due to hyperphagia, the daily metabolizable energy was 79% higher in *Pparg*$^{\Delta/\Delta}$ mice compared to controls (15.2 *vs* 8.4 kcal/day), in direct proportion to their 76% higher daily metabolic requirements (Fig. 3B).

Overall these data indicate that hyperphagia as well as intolerance to fasting in *Pparg*$^{\Delta/\Delta}$ mice result from excess energy requirements related to both urinary energy loss and hypermetabolism.

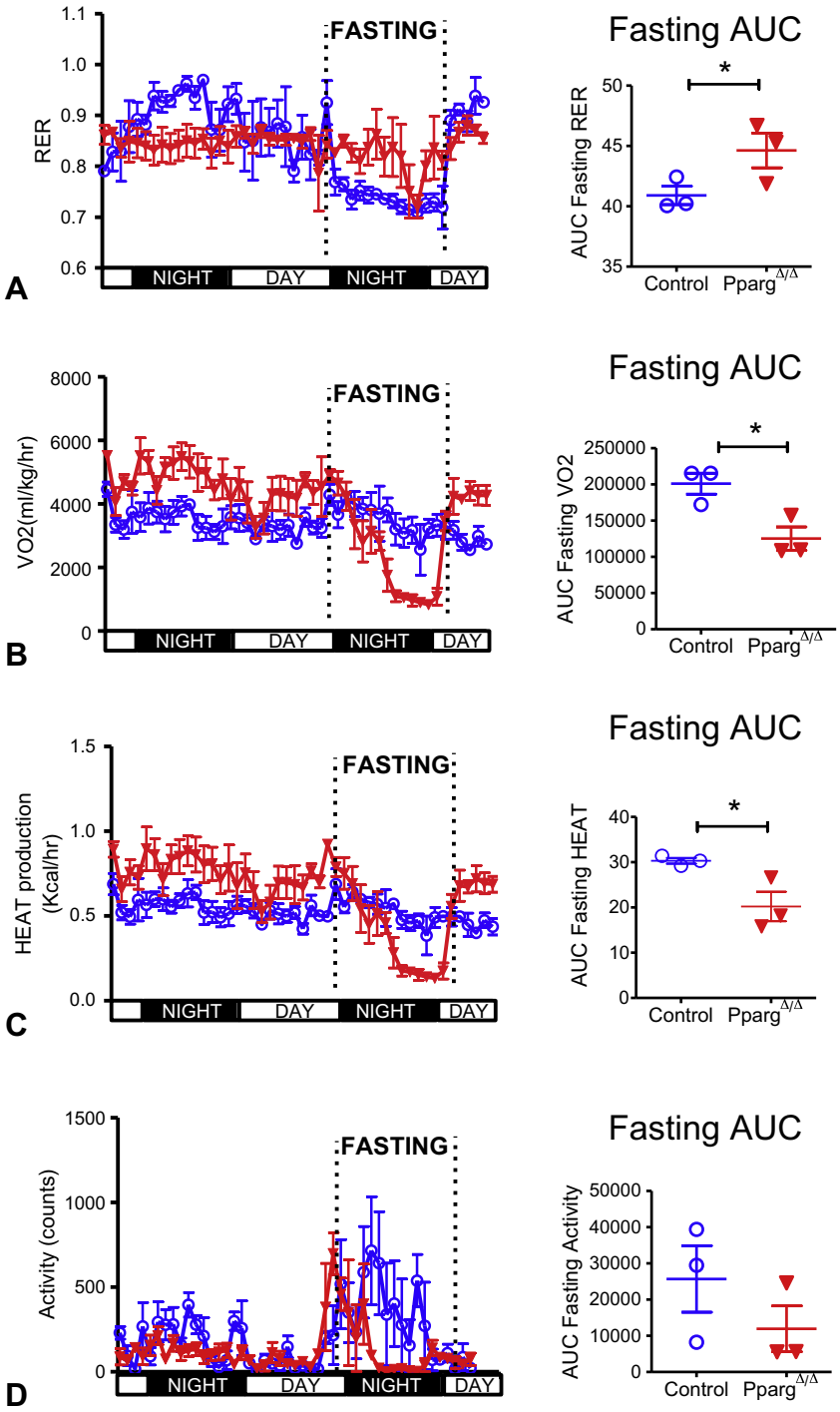

Fig. 5. Fasting-induced torpor in *Pparg*$^{\Delta/\Delta}$ mice. (A) Respiratory exchange ratio (RER), (B) oxygen consumption, (C) heat production and (D) locomotor activity in 12 weeks old control and *Pparg*$^{\Delta/\Delta}$ female mice ($N = 3$). 24 h after entering metabolic cages, mice were fasted overnight (16 h) and refed the day after. Right panels show the Areas Under the Curves (AUC) during the fasting period. Individual points and the mean ± SEM are plotted. * = $P < 0.05$ *Pparg*$^{\Delta/\Delta}$ *vs.* control littermates.

3.8. Lipid and protein metabolism alterations upon fasting in Pparg$^{\Delta/\Delta}$ *mice*

To get further insight into the impaired response to fasting, we analyzed the gene expression of key regulators in the three main pathways activated in the liver upon fasting, *i.e.* glycogenolysis, gluconeogenesis, and lipid oxidation. In the fed state, mRNA levels of *Pdk4*, a key regulator of gluconeogenesis, were normal in *Pparg*$^{\Delta/\Delta}$ mice. However, whereas *Pdk4* expression was strongly increased only after an overnight fast in controls, it was increased to similar levels already after a 5 h fast in *Pparg*$^{\Delta/\Delta}$ mice, consistent with an earlier requirement for gluconeogenesis in *Pparg*$^{\Delta/\Delta}$ mice (Fig. 7A). Along the same line, *Pgc1a*, another important regulator of gluconeogenesis which induces the expression of *Pck1*, was remarkably elevated to overnight fasted levels already in the fed and 6 h fasted states (Fig. 7B, C). Overall, these results are consistent with both the early fasting stress and the diabetic state of *Pparg*$^{\Delta/\Delta}$ mice.

PPARα, a key regulator of numerous genes involved in fatty acid oxidation upon activation by fasting, was expressed at similar levels in fed control and *Pparg*$^{\Delta/\Delta}$ mice and increased similarly after 5 h of fasting. After an overnight fast, however, PPARα expression was strikingly suppressed (Fig. 7D), along with the peroxisomal β-oxidation gene Acetyl-

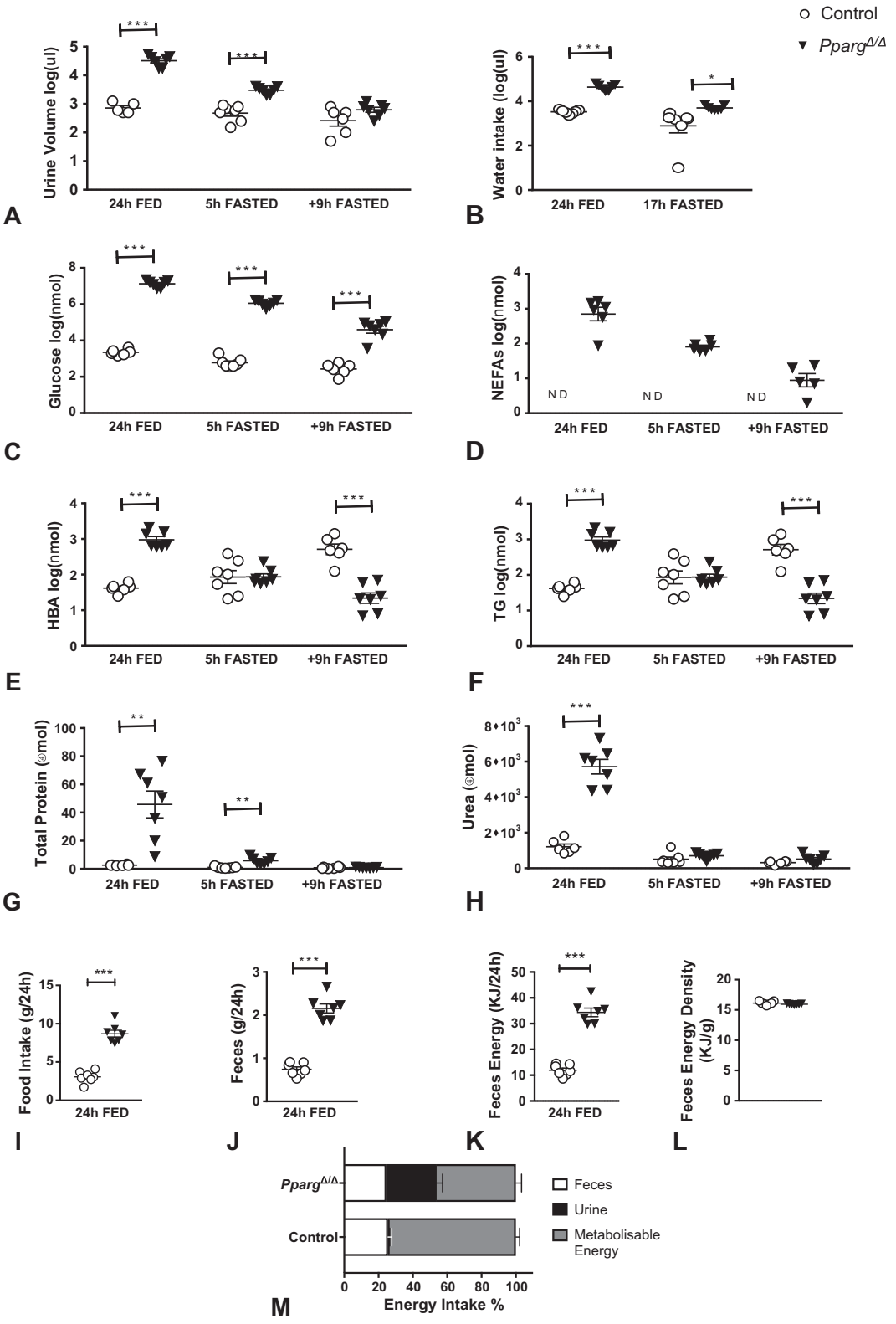

Fig. 6. Loss of substrates for energy metabolism in *Pparg*$^{\Delta/\Delta}$ mice. (A) Quantity of urine production and (B) water intake in female 15–18 weeks old *Pparg*$^{\Delta/\Delta}$ and control littermate ($N = 7$) during 24 h of *ad libitum* feeding, during the first 5 h of overnight fasting, and during the subsequent 9 h of an overnight fasting. (C–H) The total urinary loss in different substrates for energy metabolism was measured, covering the same time intervals. (C) glucose, (D) Non-Esterified Fatty Acids (NEFAs), (E) β-Hydroxybutyric acid (HBA), (F) Triglycerides (TG), (G) total proteins and (H) urea. (I) Food intake was measured along 24 h of *ad libitum* feeding. (J) Feces production in the same mice ($N = 7$) during 24 h of *ad libitum* feeding. (K, L) Total energy loss in feces over the period of 24 h was obtained by measuring the energy content of feces with calorimetric bomb (K), (L) the energy density in the feces being expressed as Joule/g. (M) The metabolisable energy was calculated by subtracting the energy lost in urine and feces to the daily energy intake. Values are expressed as percentage of the daily energy intake. In all panels, values are expressed as mean ± SEM. Due to important differences between the genotypes, the values of the panels A to F are given as log10 value. *P < 0.05, **P < 0.01, ***P < 0.0001 *Pparg*$^{\Delta/\Delta}$ *vs.* control littermates.

CoA Acytransferase 1 (*Acaa1*), and the PPARα target, ketogenic gene *Hmgcs2* (Fig. 7E–F), whereas no changes were found for the hepatic carnitine palmitoyltransferase (*Cpt1a*; Fig. 7G). Collectively, these data are in line with the accelerated catabolic state and early substrate depletion during fasting in *Pparg*$^{\Delta/\Delta}$ mice.

Given the substantial loss of lean mass upon fasting and the high urea excretion in *Pparg*$^{\Delta/\Delta}$ mice, we also explored the metabolism of aminoacids. As an index of aminoacid metabolism, we analyzed the expression of genes of the urea cycle, which detoxifies the ammonia produced by aminoacid degradation. Strikingly, four out of five genes involved in the urea cycle are significantly increased in *Pparg*$^{\Delta/\Delta}$ mice (*Got1*, *Asl*, *Ass1*, *Cps1*, but not *Oct1*; Fig. 7H–L), both in the fed and in the fasting states, suggesting that facing the metabolic inflexibility, *Pparg*$^{\Delta/\Delta}$ mice developed an adaptive glutamine utilization. Thus, the spectacular increase in lean mass in *Pparg*$^{\Delta/\Delta}$ mice may be part of an adaptive mechanism to ensure energy homeostasis.

4. Discussion

In the present report, we provide a thorough exploration of the metabolic status of mice totally deprived of adipose tissue, through constitutive systemic deletion of *Pparg*.

Consistent with the key role of PPARγ in adipose tissue formation, *Pparg*$^{\Delta/\Delta}$ mice are totally lipodystrophic, with no structured or

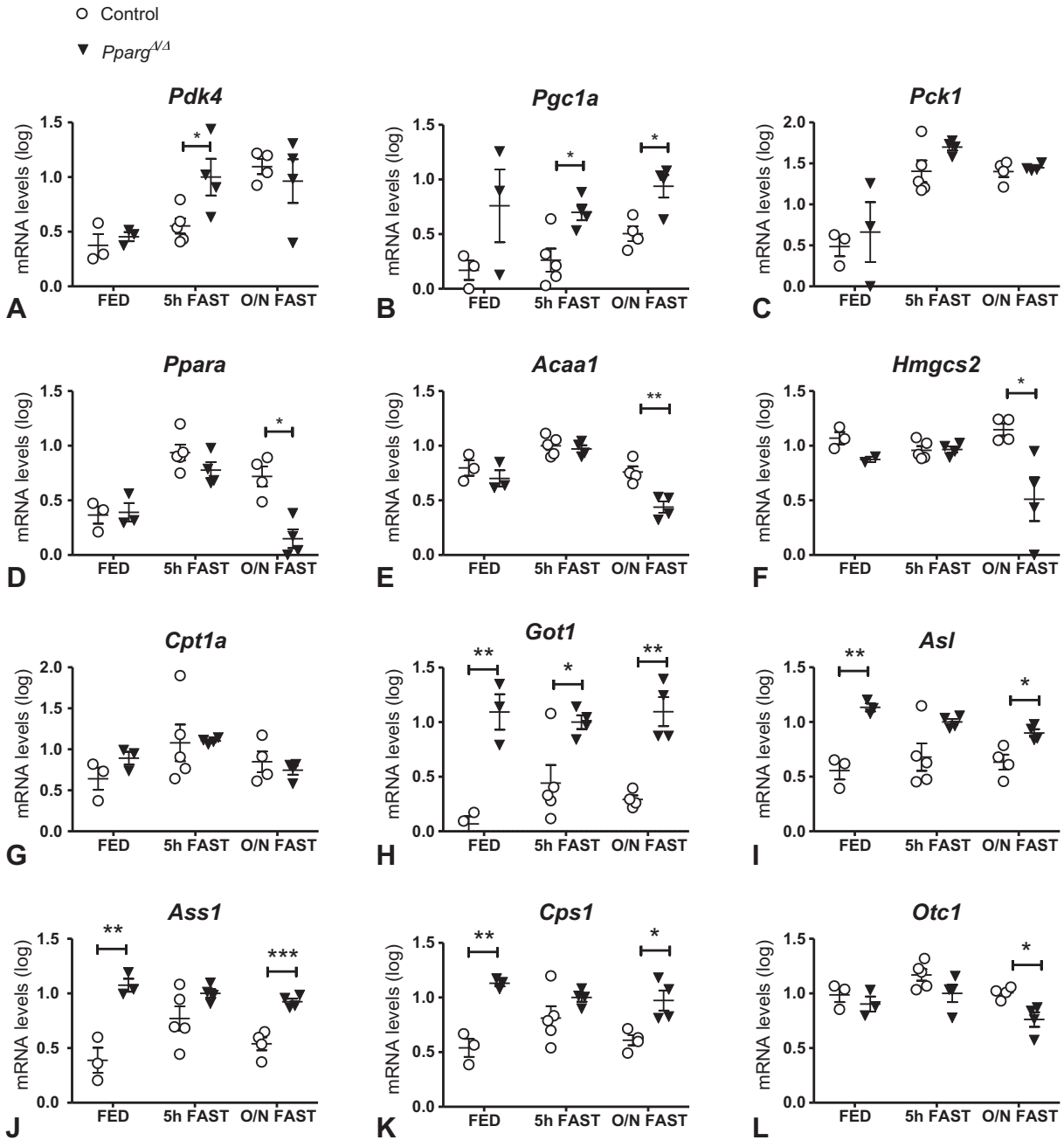

Fig. 7. Lipid and protein metabolism alterations upon fasting in *Pparg*$^{\Delta/\Delta}$ mice. Gene expression levels of (A) Pyruvate Dehydrogenase Kinase 4 (*Pdk4*), (B) Peroxisome Proliferator-Activated Receptor gamma coactivator 1 alpha (*Pgc1a*), (C) Phosphoenolpyruvate Carboxykinase 1 (*Pck1*), (D) Peroxisome Proliferator-Activated Receptor alpha (*Ppara*), (E) Acetyl-CoA Acyltransferase 1 (*Acaa1*), (F) 3-Hydroxy-3-Methylglutaryl-CoA Synthase 2 (*Hmgcs2*), (G) Carnitine Palmitoyltransferase (*Cpt1a*), (H) Glutamic-oxaloacetic transaminase (*Got1*), (I) Arginosuccinate Lyase (*Asl*), (J) Argininosuccinate Synthase 1 (*Ass1*), (K) Carbamoyl-Phosphate Synthase 1 (*Cps1*), (L) Ornithine Carbamoyltransferase 1 (*Otc1*) were measured in liver from control and *Pparg*$^{\Delta/\Delta}$ mice ($N = 3$–5) fed, or upon 5 h and over-night fasting. Individual data and the mean ± SEM are represented. All values are given as log10 values. *P < 0.05, **P < 0.01, ***P < 0.0001 *Pparg*$^{\Delta/\Delta}$ *vs.* control littermates.

unstructured fat depots, except in the liver where steatosis is present. In contrast, these mice display an important increase in lean mass, accompanied by organomegalia. As a consequence of the lipoatrophy, *Pparg*$^{\Delta/\Delta}$ develop severe type-2 diabetes, characterized by hyperglycemia, hyperinsulinemia, polyphagia, polydispsia and polyuria. In depth metabolic analyses reveal four major findings: first, a remarkable metabolic inflexibility in both *ad libitum* fed state and fed/fasted/refed transitions, with severe intolerance to fasting; second, a massive urinary loss of energy in form of glucose, lipids and proteins; third, a hypermetabolic phenotype related to the increase in lean mass but not to insulation defects, which, together with urinary energy loss, contributes to the major hyperphagia of *Pparg*$^{\Delta/\Delta}$ mice; fourth, an activation of the urea cycle, suggesting an adaptive mechanism to ensure energy homeostasis in absence of adipose tissue.

The exploration of the effects of systemic ablation of PPARγ is an important step towards understanding how distinct PPARγ activities are integrated in the whole organism, which might be relevant in a clinical perspective considering that PPARγ agonists (TZDs) were the treatment of choice for type-2 diabetes before their use was restricted due to serious side effects. Here we provide the first study of the effects of a full, systemic ablation of PPARγ. Interestingly, the metabolic phenotype carried by *Pparg*+/− and *Pparg*$^{\Delta/\Delta}$ mice is quite different, with *Pparg*+/− being protected against insulin-resistance, rather than being more prone to develop this metabolic disorder, as it is seen in *Pparg*$^{\Delta/\Delta}$ [30,31]. The lack of the *Pparg* gene dosage effect on the metabolic phenotype is likely due to the total absence of adipose tissue in *Pparg*$^{\Delta/\Delta}$ compared to a diminished propensity to increase upon high fat diet in *Pparg*+/−. The total lack of adipose tissue in the former is bringing its load of metabolic consequences, which make *Pparg*$^{\Delta/\Delta}$ mice a more powerful model to understand fundamental aspects of energy homeostasis in lipoatrophy rather than to disentangle cell-autonomous effects of PPARγ.

To the best of our knowledge, *Pparg*$^{\Delta/\Delta}$ mice are the first available model fully deprived of WAT and BAT throughout life. A-ZIP/F-1 mice, one of the first models resembling the Berardinelli-Seip syndrome of generalized lypodystrophy, had a WAT reduction of almost 99% but presented a normal BAT at birth that shrank with age [32]. Mice lacking seipin (*Bscl2*), the gene whose mutation is one of the causes of the Berardinelli-Seip syndrome, have residual fat pads in visceral and subcutaneous locations, before the age of 6 months [33–35]. Recently, another model of severe lipoatrophy was obtained through Adipoq-Cre mediated PPARγ deletion (PPARγFKO). However, while 8 days old PPARγFKO mice had virtually no BAT, some inguinal and interscapular mature adipocytes were still detectable [17]. Therefore, *Pparg*$^{\Delta/\Delta}$ mice represent a unique model to study the systemic and local effects of total lack of fat tissue [24].

Several observations done in *Pparg*$^{\Delta/\Delta}$ mice also illustrate some limitations of the interpretation of results obtained *via* tissue- or cell-specific PPARγ gene deletion. As an example, PPARγ mutant mice presented hepatomegaly and steatosis, which, at first sight, could seem unexpected, especially considering that PPARγ is commonly upregulated in the steatotic liver. Furthermore, specific liver PPARγ deletion was shown to ameliorate hepatosteatosis in both A-ZIP/F-1 and diet-induced obese mice [36,37], while TZD treatment reduced plasma glucose and triglycerides in liver-specific and muscle-specific PPARγ-deleted mice [36]. However, the phenotype observed in *Pparg*$^{\Delta/\Delta}$ mice demonstrates that, in the context of full deprivation of fat, PPARγ is not required for lipid droplet formation in hepatocytes.

A second interesting aspect of *Pparg*$^{\Delta/\Delta}$ mice was enhanced beta cell mass and insulin production in face of hyperglycemia. However the relative contribution of PPARγ deletion in the context of the diabetic compensation remains unclear. Rosen et al. showed that loss of PPARγ in pancreatic β-cells was associated with a hyperplastic response, but no metabolic abnormalities [38]. More recently, a FoxO1/PPARγ mediated network was proposed as a core element for β-cell compensation and failure in response to metabolic stress [39]. Overall our study shows that lack of PPARγ does not lead to defects in pancreatic beta cell function.

Lipodystrophic *Pparg*$^{\Delta/\Delta}$ mice showed a spectacular increase in the lean mass. This phenotype is likely related to lipodystrophy rather than to PPARγ deletion, as it was also reported in A-ZIP/F-1 mice [32]. The causal relationship between lipodystrophy and increased lean mass is however unknown.

Upon fasting aminoacids, mainly coming from catabolic wasting of lean mass, are used for gluconeogenesis. In *Pparg*$^{\Delta/\Delta}$ mice, the expression of genes of the urea cycle was considerably increased in both *ad libitum* fed and fasted states. Accordingly, *Pparg*$^{\Delta/\Delta}$ mice display a rise in the 24 h urea excretion in the fed state. This suggests an increase in aminoacid metabolism, likely related to hyperphagia-associated higher protein intake and possibly also to a higher mobilization of endogenous proteins for metabolism in the post-absorptive state. During fasting, however, there was no more elevation of urea excretion, despite the higher expression of urea cycle genes, possibly due to an exhaustion of the substrates easily available. In this context, the fact that *Pparg*$^{\Delta/\Delta}$ mice lose twice as much lean mass as controls during fasting may be due in part to the higher urinary protein loss. Overall it is tempting to speculate that the increased lean mass in *Pparg*$^{\Delta/\Delta}$ mice is a metabolic adaptation to lipodystrophy and its complications.

Pparg$^{\Delta/\Delta}$ mice display an intriguing hypermetabolism that seems to be mainly but not entirely explained by the increase in lean, metabolically active mass. At first sight, this might suggest that other (*e.g.* cell-autonomous) mechanisms might account for part of the hypermetabolism. However, it may more likely reflect a limitation of normalization to lean mass – which relies on the assumption that the mass-specific metabolic rate remains constant when lean mass changes. Indeed, this assumption is not true in *Pparg*$^{\Delta/\Delta}$ mice that show a disproportionately high enlargement of the liver compared to the total increase in lean mass. Moreover, liver has, together with the muscle, the highest mass-specific metabolic rate [40] and is the organ which correlates best to basal metabolic rate [41]. Thus the hypermetabolism in *Pparg*$^{\Delta/\Delta}$ mice is in many respects unlike other hypermetabolic clinical situations such as HIV-associated lipodystrophy [42], burn injury or cancer, which are associated with sarcopenia or cachexia, particularly in chronic situations.

Metabolic inflexibility in *Pparg*$^{\Delta/\Delta}$ mice - as operationally defined by decreased variations in the respiratory quotient during nutritional changes, independently of the underlying mechanisms - is suggested by the disappearance of physiological oscillations of RER in the *ad libitum* state, as well as by the absence of RER drop to 0.7 during transitions from *ad libitum* to fasted and rebound. Although the urinary loss of glucose (and to a lesser extent of ketone bodies) in *Pparg*$^{\Delta/\Delta}$ mice may artificially lower the RER in the fed state, thereby flattening its circadian pattern, this would not explain why upon fasting the RER does not rapidly drop down to expected fasted values. The lack of organized fat tissue under hormonal control of lipolysis by insulin and catecholamines is one possible explanation for this metabolic inflexibility, unlike in type 2 diabetic patients where metabolic inflexibility rather reflects an impaired insulin axis [43–45].

Upon fasting, *Pparg*$^{\Delta/\Delta}$ mice rapidly deplete their body energy stores and enter torpor, a hypometabolic, hibernation-like state. Although lipodystrophy *per se* plays a major role, it is interesting to note that leptin deficiency has been described as a possible actor for the entry in torpor-like state upon fasting, as observed in both obese *ob*/*ob* mice and lipodystrophic A-ZIP/F-1 mice [46].

Several intriguing questions remain, such as how is feeding regulated in *Pparg*$^{\Delta/\Delta}$ mice in absence of leptin, and to what extent is the absence of leptin relevant to the increase in body weight and lean mass compared to controls beyond 8 weeks of age.

More generally, this discussion highlights the complexity of the metabolic interplay between lack of adipose tissue, increased lean mass, hypermetabolism, hyperphagia and metabolic inflexibility. A molecular and system approach to understand the possible mechanisms of

adaptation would provide some clues on fundamental aspects of energy metabolism, as well as on related questions of clinical relevance.

Author contributions

FG conceived the study, designed the experimental plan, performed most of the experiments, analyzed data and wrote the manuscript. CW performed most of the experiments. LQ and CS participated in the initial elaboration of the project. JGD participated to the indirect calorimetry experiments. BT participated to the initial experiments and analyzed data. MS participated to the fasting-refeeding experiments. FP designed the experimental plan, contributed to indirect calorimetry and metabolic cages experiments, analyzed data and wrote the manuscript. BD conceived and supervised the study, and wrote the manuscript. All authors read and edited the manuscript.

Funding

This work was supported by grants to BD from the Swiss National Science Foundation (3100AO-120633/1), the Etat de Vaud, and the Faculty of Biology and Medicine of the University of Lausanne. LQ was a recipient of a FEBS postdoctoral fellow.

Conflict of interest/financial disclosure statement

None.

Acknowledgements

The authors would like to thank Patrick C. Even for his critical reading of the manuscript. We also thank Catherine Moret (Center for Integrative Genomics, Lausanne) for her advices in the histology, Maude Delacombaz (Center for Integrative Genomics, Lausanne) for her help in the histological preparations, Anabela Rebelo Pimentel, Guy Niederhauser and Gilles Willemin (Mouse Metabolic Evaluation Facility, MEF, University of Lausanne) for their help in metabolic studies, and Katarina Hausherr and Fabienne Lammers from the genotyping facility.

Appendix A. Supplementary data

Supplementary data to this article can be found online at https://doi.org/10.1016/j.metabol.2019.03.003.

References

[1] Grundy SM, Brewer Jr HB, Cleeman JI, Smith Jr SC, Lenfant C. Definition of metabolic syndrome: report of the National Heart, Lung, and Blood Institute/American Heart Association conference on scientific issues related to definition. Circulation 2004;109:433–8.
[2] Guo S. Insulin signaling, resistance, and the metabolic syndrome: insights from mouse models into disease mechanisms. J Endocrinol 2014;220:T1–T23.
[3] Hajer GR, van Haeften TW, Visseren FL. Adipose tissue dysfunction in obesity, diabetes, and vascular diseases. Eur Heart J 2008;29:2959–71.
[4] Torres-Leal FL, Fonseca-Alaniz MH, Rogero MM, Tirapegui J. The role of inflamed adipose tissue in the insulin resistance. Cell Biochem Funct 2010;28:623–31.
[5] Caputo T, Gilardi F, Desvergne B. From chronic overnutrition to metaflammation and insulin resistance: adipose tissue and liver contributions. FEBS Lett 2017;591:3061–88.
[6] Rochford JJ. Molecular mechanisms controlling human adipose tissue development: insights from monogenic lipodystrophies. Expert Rev Mol Med 2010;12:e24.
[7] Garg A. Clinical review#: lipodystrophies: genetic and acquired body fat disorders. J Clin Endocrinol Metab 2011;96:3313–25.
[8] Samuel VT, Petersen KF, Shulman GI. Lipid-induced insulin resistance: unravelling the mechanism. Lancet 2010;375:2267–77.
[9] Asrih M, Jornayvaz FR. Diets and nonalcoholic fatty liver disease: the good and the bad. Clin Nutr 2014;33:186–90.
[10] Virtue S, Vidal-Puig A. Adipose tissue expandability, lipotoxicity and the metabolic syndrome–an allostatic perspective. Biochim Biophys Acta 2010;1801:338–49.
[11] Rosen ED, Sarraf P, Troy AE, Bradwin G, Moore K, Milstone DS, et al. PPAR gamma is required for the differentiation of adipose tissue in vivo and in vitro. Mol Cell 1999;4:611–7.
[12] Imai T, Takakuwa R, Marchand S, Dentz E, Bornert JM, Messaddeq N, et al. Peroxisome proliferator-activated receptor gamma is required in mature white and brown adipocytes for their survival in the mouse. Proc Natl Acad Sci U S A 2004;101:4543–7.
[13] Gelman L, Feige JN, Desvergne B. Molecular basis of selective PPARgamma modulation for the treatment of type 2 diabetes. Biochim Biophys Acta 2007;1771:1094–107.
[14] Desvergne B, Michalik L, Wahli W. Be fit or be sick: peroxisome proliferator-activated receptors are down the road. Mol Endocrinol 2004;18:1321–32.
[15] Hegele RA. Lessons from human mutations in PPARgamma. Int J Obes (Lond) 2005;29(Suppl. 1):S31–5.
[16] Medina-Gomez G, Gray SL, Yetukuri L, Shimomura K, Virtue S, Campbell M, et al. PPAR gamma 2 prevents lipotoxicity by controlling adipose tissue expandability and peripheral lipid metabolism. PLoS Genet 2007;3:e64.
[17] Wang F, Mullican SE, DiSpirito JR, Peed LC, Lazar MA. Lipoatrophy and severe metabolic disturbance in mice with fat-specific deletion of PPARgamma. Proc Natl Acad Sci U S A 2013;110:18656–61.
[18] Hevener AL, He W, Barak Y, Le J, Bandyopadhyay G, Olson P, et al. Muscle-specific Pparg deletion causes insulin resistance. Nat Med 2003;9:1491–7.
[19] Odegaard JI, Ricardo-Gonzalez RR, Goforth MH, Morel CR, Subramanian V, Mukundan L, et al. Macrophage-specific PPARgamma controls alternative activation and improves insulin resistance. Nature 2007;447:1116–20.
[20] Barak Y, Nelson MC, Ong ES, Jones YZ, Ruiz-Lozano P, Chien KR, et al. PPAR gamma is required for placental, cardiac, and adipose tissue development. Mol Cell 1999;4:585–95.
[21] Nadra K, Quignodon L, Sardella C, Joye E, Mucciolo A, Chrast R, et al. PPARgamma in placental angiogenesis. Endocrinology 2010;151:4969–81.
[22] Duan SZ, Ivashchenko CY, Whitesall SE, D'Alecy LG, Duquaine DC, Brosius III FC, et al. Hypotension, lipodystrophy, and insulin resistance in generalized PPARgamma-deficient mice rescued from embryonic lethality. J Clin Invest 2007;117:812–22.
[23] Hayashi S, Lewis P, Pevny L, McMahon AP. Efficient gene modulation in mouse epiblast using a Sox2Cre transgenic mouse strain. Gene Expr Patterns 2002;2:93–7.
[24] Sardella C, Winkler C, Quignodon L, Hardman JA, Toffoli B, Giordano Attianese GMP, et al. Delayed hair follicle morphogenesis and hair follicle dystrophy in a lipoatrophy mouse model of Pparg total deletion. J Invest Dermatol 2018;138:500–10.
[25] Gilardi F, Giudici M, Mitro N, Maschi O, Guerrini U, Rando G, et al. LT175 is a novel PPARalpha/gamma ligand with potent insulin-sensitizing effects and reduced adipogenic properties. J Biol Chem 2014;289:6908–20.
[26] Tontonoz P, Spiegelman BM. Fat and beyond: the diverse biology of PPARgamma. Annu Rev Biochem 2008;77:289–312.
[27] Wilson A, Fu H, Schiffrin M, Winkler C, Koufany M, Jouzeau J-Y, et al. Lack of adipocytes alters hematopoiesis in lipodystrophic mice. Front Immunol 2018;9:2573. https://doi.org/10.3389/fimmu.2018.02573 eCollection 2018.
[28] Dammone G, Karaz S, Lukjanenko L, Winkler C, Sizzano F, Jacot G, et al. PPARgamma controls ectopic adipogenesis and cross-talks with myogenesis during skeletal muscle regeneration. Int J Mol Sci 2018;19.
[29] Toffoli B, Gilardi F, Winkler C, Soderberg M, Kowalczuk L, Arsenijevic Y, et al. Nephropathy in Pparg-null mice highlights PPARgamma systemic activities in metabolism and in the immune system. PLoS One 2017;12:e0171474.
[30] Kubota N, Terauchi Y, Miki H, Tamemoto H, Yamauchi T, Komeda K, et al. PPAR gamma mediates high-fat diet-induced adipocyte hypertrophy and insulin resistance. Mol Cell 1999;4:597–609.
[31] Rieusset J, Touri F, Michalik L, Escher P, Desvergne B, Niesor E, et al. A new selective peroxisome proliferator-activated receptor gamma antagonist with antiobesity and antidiabetic activity. Mol Endocrinol 2002;16:2628–44.
[32] Moitra J, Mason MM, Olive M, Krylov D, Gavrilova O, Marcus-Samuels B, et al. Life without white fat: a transgenic mouse. Genes Dev 1998;12:3168–81.
[33] Cui X, Wang Y, Tang Y, Liu Y, Zhao L, Deng J, et al. Seipin ablation in mice results in severe generalized lipodystrophy. Hum Mol Genet 2011;20:3022–30.
[34] Prieur X, Dollet L, Takahashi M, Nemani M, Pillot B, Le May C, et al. Thiazolidinediones partially reverse the metabolic disturbances observed in Bscl2/seipin-deficient mice. Diabetologia 2013;56:1813–25.
[35] Chen W, Chang B, Saha P, Hartig SM, Li L, Reddy VT, et al. Berardinelli-seip congenital lipodystrophy 2/seipin is a cell-autonomous regulator of lipolysis essential for adipocyte differentiation. Mol Cell Biol 2012;32:1099–111.
[36] Moran-Salvador E, Lopez-Parra M, Garcia-Alonso V, Titos E, Martinez-Clemente M, Gonzalez-Periz A, et al. Role for PPARgamma in obesity-induced hepatic steatosis as determined by hepatocyte- and macrophage-specific conditional knockouts. FASEB J 2011;25:2538–50.
[37] Gavrilova O, Haluzik M, Matsusue K, Cutson JJ, Johnson L, Dietz KR, et al. Liver peroxisome proliferator-activated receptor gamma contributes to hepatic steatosis, triglyceride clearance, and regulation of body fat mass. J Biol Chem 2003;278:34268–76.
[38] Rosen ED, Kulkarni RN, Sarraf P, Ozcan U, Okada T, Hsu CH, et al. Targeted elimination of peroxisome proliferator-activated receptor gamma in beta cells leads to abnormalities in islet mass without compromising glucose homeostasis. Mol Cell Biol 2003;23:7222–9.
[39] Gupta D, Leahy AA, Monga N, Peshavaria M, Jetton TL, Leahy JL. Peroxisome proliferator-activated receptor gamma (PPARgamma) and its target genes are downstream effectors of FoxO1 protein in islet beta-cells: mechanism of beta-cell compensation and failure. J Biol Chem 2013;288:25440–9.
[40] Rolfe DF, Brown GC. Cellular energy utilization and molecular origin of standard metabolic rate in mammals. Physiol Rev 1997;77:731–58.
[41] Mitchell SE, Tang Z, Kerbois C, Delville C, Derous D, Green CL, et al. The effects of graded levels of calorie restriction: VIII. Impact of short term calorie and protein

restriction on basal metabolic rate in the C57BL/6 mouse. Oncotarget 2017;8:17453–74.
[42] Kosmiski LA, Bessesen DH, Stotz SA, Koeppe JR, Horton TJ. Short-term energy restriction reduces resting energy expenditure in patients with HIV lipodystrophy and hypermetabolism. Metabolism 2007;56:289–95.
[43] Kelley DE, Mandarino LJ. Fuel selection in human skeletal muscle in insulin resistance: a reexamination. Diabetes 2000;49:677–83.
[44] Galgani JE, Moro C, Ravussin E. Metabolic flexibility and insulin resistance. Am J Physiol Endocrinol Metab 2008;295:E1009–17.
[45] Faerch K, Vaag A. Metabolic inflexibility is a common feature of impaired fasting glycaemia and impaired glucose tolerance. Acta Diabetol 2011;48:349–53.
[46] Gavrilova O, Leon LR, Marcus-Samuels B, Mason MM, Castle AL, Refetoff S, et al. Torpor in mice is induced by both leptin-dependent and -independent mechanisms. Proc Natl Acad Sci U S A 1999;96:14623–8.